

Magnetization reversal of giant perpendicular magnetic anisotropy at the magnetic-phase transition in FeRh films on MgO

Dorj Odkhuu*

Department of Physics, Incheon National University, Incheon 406-772, Korea

(Received 27 June 2015; revised manuscript received 8 January 2016; published 8 February 2016)

Based on first-principles calculations, we demonstrate that substitutions of transition metals Ru and Ir, neighboring and same group elements in the periodic table, for the Rh site in the vicinity of surface can induce a substantially large perpendicular magnetic anisotropy (PMA), up to an order of magnitude of 20 erg/cm², in FeRh films on MgO. The main driving mechanism for this huge PMA is the interplay between the d_{xy} and $d_{x^2-y^2}$ orbital states of the substitutional 4d and 5d transition metal atoms with large spin-orbit coupling. Further investigations demonstrate that magnetization direction of PMA undergoes a transition into an in-plane magnetization at the antiferromagnet \rightarrow ferromagnet phase transition, which provides a viable route for achieving large and switchable PMA associated with the magnetic-phase transition in antiferromagnet spintronics.

DOI: [10.1103/PhysRevB.93.064412](https://doi.org/10.1103/PhysRevB.93.064412)

I. INTRODUCTION

Spin-orbit coupling (SOC) interaction driven phenomena such as magnetic anisotropy (MA), Rashba-type interactions, or topological insulators lead to the emergence of intriguing physics as well as advances in practical applications. In particular, large perpendicular MA (PMA), magnetization direction normal to the film plane, offers great opportunities in recent memory technologies such as spin transfer torque effect (STT) [1]. To date, the large PMA has been demonstrated in several transition-metal [ferromagnet|insulating (TM|FM|I) heterostructures; the most successful example is Ta|CoFeB|MgO [2]. However, magnetization switching of a FM layer in STT requires a large spin-polarized tunneling current, and thus energy consuming.

There have been intense research efforts to reduce the current density while still retaining thermal stability. The thermal stability factor Δ is maintained by the large PMA, through $\Delta = KV/k_B T$, where K , V , k_B , and T are anisotropy, volume, Boltzmann constant, and temperature, respectively [3]. And the critical current I_c is expressed as [4]

$$I_c = \frac{2e}{\hbar} \frac{\alpha}{\eta} M_s V (H_k + 2\pi M_s), \quad (1)$$

where α , M_s , and H_k represent Gilbert damping coefficient, saturation magnetization, and the Stoner-Wolfarth switching field; η is the spin polarization factor. The most materials proposed for memory applications are soft magnets, i.e., $H_k \ll M_s$, thus $I_c \sim M_s^2 V$. A small V is favored to lower I_c , which is, on the other hand, detrimental for the thermal stability. Therefore, exploration for low magnetization materials with large PMA would be one favorable direction to minimize I_c and maximize Δ at the same time.

Ideal material that can fulfill the aforementioned prerequisites could be an antiferromagnet (AFM) metal [5]. This furthermore yields negligible stray fields and is also investitive to the strong magnetic fields [6,7]. While the explorations of the

occurrence of the phase transition in B2-ordered FeRh alloys from AFM to FM phase at around 350 K have been a long-standing subject of both theoretical [8–10] and experimental studies [11,12], there have been recently growing interests in FeRh films deposited on MgO [6,7,13] and BaTiO₃ [14,15] as a potential candidate for AFM-based spintronics including magnetoelectric [14,15], magnetocaloric [16], and heat-assisted magnetic recording [17], owing to rich emergent phenomena such as thermal and electric-field controls of magnetic-phase transition [14,15] and room-temperature bistable AFM formation [6,7]. In recent electron Mossbauer spectroscopy experiments, the spin switching of magnetization has been also demonstrated during the the AFM \rightarrow FM transition in FeRh |MgO films [13].

In recent studies, on the other hand, the role of 4d and 5d orbitals on PMA is addressed and cannot be ignored because of their inherently larger SOC than conventional 3d metals [18–20]. Instability of the Rh magnetic moment [9,21] and spin-wave excitation [22] were also proposed to be responsible for the AFM \rightarrow FM transition of FeRh. Furthermore, several experimental studies have consistently reported that the small amounts of TM substitutions (Ru, Pd, Ir, and Pt) for the Rh site in FeRh can modulate the transition temperature over a wide range, 100–600 K (Ref. [23] and references therein). From these facts, the presence of TMs including Rh in FeRh could be an essential ingredient for the magnetic-phase transition and transition driven magnetic properties, which urges further intriguing and valuable explorations that account for the decisive role of 4d and 5d TMs on magnetic properties of FeRh films.

In this article we propose a promising approach that leads to the huge PMA by substituting neighboring and same group elements of Ru and Ir for the Rh site in the vicinity of surface in FeRh |MgO. The underlying mechanism is the interplay between the d_{xy} and $d_{x^2-y^2}$ states of the substitutional large spin-orbit 4d and 5d orbitals. We further demonstrate that the magnetization can change its direction from the PMA to an in-plane magnetization at the AFM \rightarrow FM phase transition. Moreover, the presence of Rh/substitutional atoms (MgO) at the surface (interface) enhances PMA greatly and ignites FM instability therein.

*odkhuu@inu.ac.kr

II. COMPUTATIONAL DETAILS

Density functional calculations were performed using the Vienna *ab initio* simulation package (VASP) [24], and exchange-correlation interactions were described with the PBE-type generalized gradient approximation (GGA) [25]. Energy cutoff 500 eV and $11 \times 11 \times 1$ k mesh were imposed for the ionic relaxation, where forces acting on atoms were less than 10^{-2} eV/Å. SOC is included using the second-variation method employing the scalar-relativistic eigenfunctions of the valence states [26]. Total MA energy (MAE) is calculated from the total energy difference when the magnetization directions are on the xy plane and along the z axis, $\text{MAE} = \frac{1}{a^2}(E^{\parallel} - E^{\perp})$, where a is the in-plane lattice constant, so that positive MAE stands for the preferable direction of magnetization normal to the film plane, i.e., PMA. We also calculate atom resolved MAE by the energy contribution to the total MAE from each atomic site in the SOC matrix elements, as shown in Eq. (2) in the following section. To ensure convergence of MAE value, different k points, up to $31 \times 31 \times 1$, were sampled for the different thicknesses of FeRh films.

We consider the 2–6 unit cell (u.c.) layers of FeRh films on four atomic layers of MgO, as a model geometry shown in Fig. 1(a). The Fe atoms were placed atop of O atoms at the interface. The experimental lattice constant (4.212 Å) of MgO was adopted for the in-plane lattice of supercells, which is matched to the optimized bulk lattices of AFM (type II) and FM FeRh within 0.5% and 1.1%, respectively. Hereafter, the number of FeRh u.c. layers (n) are denoted in subscripts $(\text{FeRh})_n$ and the TM substitutional layer at the topmost surface Rh (l th Rh layer away from the surface) is labeled as S ($S - l$). The four distinct magnetic configurations for each n were taken into account so as to identify the most stable structure: entire AFM-II and FM, and reconstructed AFM-II with FM layer at the interface, denoted as FM(I), and surface, denoted as FM(S) [Fig. 1(a)]. The other spin-antiparallel magnetic structures, i.e., type I (or A-AFM) and type III (or C-AFM), have been excluded in the present study since they were found to have relatively high energies than the AFM-II and FM phases [27].

III. RESULTS AND DISCUSSION

The relative energies of the FM, FM(I), and FM(S) magnetic structures with respect to the AFM-II are shown in Fig. 1(b) for Ir substitution at the S site of FeRh|MgO films with $n = 2-6$. While the AFM-II is the most stable phase when $n \leq 3$, the total energy of the FM(I) tends to coincide with that of the AFM-II for the larger n . The occurrence of ferromagnetism at the interface can be addressed twofold: Fe $3d$ -O $2p$ hybridization and broken Goodenough-Kanamori-Anderson (GKA) rule. In the MgO-free or center layers, the stability of AFM-II over the FM phase (relative energy of AFM-II with respect to the FM tends to achieve its bulk value, denoted as dashed line, at $n > 6$) is explained by the GKA superexchange interaction between next-to-nearest neighbor magnetic ions through a nonmagnetic mediation (Fe-Rh-Fe). In the GKA rule, the Fe atoms on the [111] and [110] directions prefer the spin-antiparallel and spin-parallel couplings, respectively, owing to the Fe-Rh-Fe angles of 180° and near 90° [27].

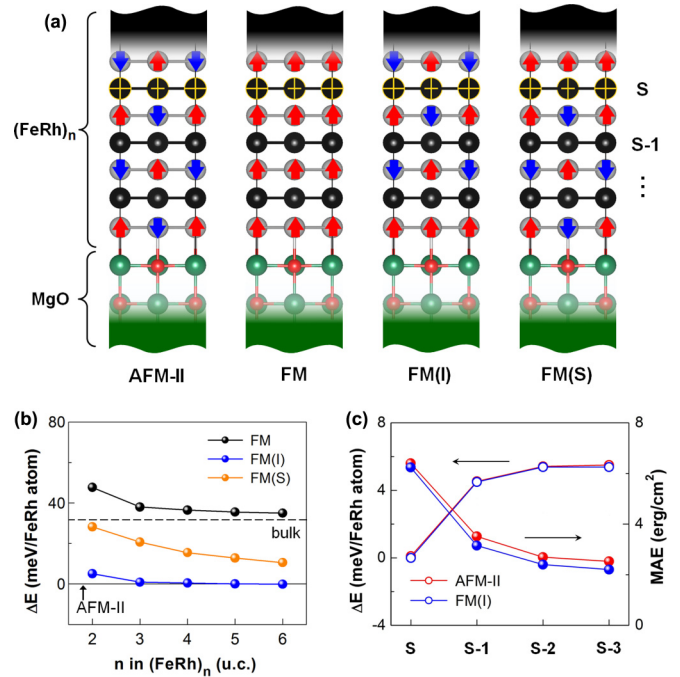


FIG. 1. (a) Atomic structures of the TM-substituted FeRh|MgO films for the different magnetic configurations. Left to right: entire AFM-II, entire FM, reconstructed AFM-II with the FM at the interface FM(I), and reconstructed AFM-II with FM at the surface FM(S). Red upward and blue downward arrows indicate the spin orientation of Fe atoms. n in subscript denotes the number of FeRh unit cell layers and S ($S - l$) denotes the topmost Rh layer (l th Rh layer away from the surface). The atomic species are denoted in spheres with different colors: Larger gray, black, cross black, green, and smaller red spheres are the Fe, Rh, TM, Mg, and O atoms, respectively. (b) Relative energy as a function of n for the FM, FM(I), and FM(S) of the Ir-substituted FeRh|MgO with respect to the AFM-II phase. The horizontal dashed line indicates the energy difference between the AFM-II and FM phases in bulk FeRh. (c) Relative energy ΔE (open symbols) and magnetic anisotropy energy MAE (filled symbols) for the different substitutional layers, from S to the center $S - 3$ layer, of the most stable AFM-II and FM(I) phases of the Ir-substituted FeRh|MgO at $n = 6$. Total energy corresponding to the S th layer substitution is taken as reference energy.

Next, with the selected thickness of FeRh films at $n = 6$, the preferred site of substitutional layer is determined for the low-temperature AFM-II and FM(I) phases, in which the substitutional atoms are alternatively replaced for the Rh layer from the outermost surface S to a center layer $S - l$. As shown in Fig. 1(c), for both magnetic configurations the relative energy $E(S - l) - E(S)$ increases gradually with l , indicating the stabilization of doping elements in the vicinity of surface. There have been several recent experimental reports on the evidence of the interfacial FM layer and surface-site doping in TM-capped FeRh|MgO films, as mentioned previously [23,28,29]. The calculated MAE of the AFM-II and FM(I) phases are also shown in Fig. 1(c) for each substitutional layer, from S to $S - 3$. While the substitutional atoms are stabilized near the surface, the MAE increases dramatically as the substitutional layer towards to the surface. In particular, the presence of substitutional Ir atoms at the most stable S site

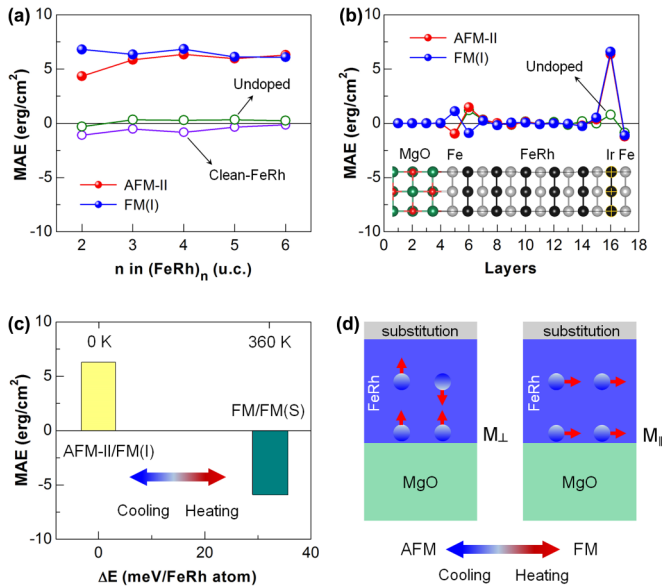


FIG. 2. (a) Thickness dependent total and (b) layer-resolved MAE for the low-temperature AFM-II (filled red) and FM(I) phases (filled blue) of the Ir-substituted FeRh|MgO. The corresponding results for the undoped FeRh films with and without MgO are presented in open green and violet circles, respectively. (b) Layer-decomposed MAE for AFM-II (red) and FM(I) (blue) of the Ir-substituted FeRh|MgO when $n = 6$. The corresponding results for the undoped films are also presented in open green. (c) MAE against the relative energy for the low-temperature AFM-II and high-temperature FM phases. (d) Schematic representation for the switching of spin direction from/to the perpendicular (left), PMA, to/from the in-plane magnetization (right) during the AFM \rightarrow FM phase transition.

leads to a very large MAE of about 6.4 erg/cm², the positive value in magnitude of which indicates that the favorable direction of magnetization is normal to the film plane, i.e., PMA.

Figure 2(a) shows the calculated MAE as a function of n for the AFM-II and FM(I) phases of FeRh|MgO with the S -site Ir substitution. For comparison, those of the substitution-free FeRh|MgO and clean FeRh films are also presented. As a generic, the saturation behavior of MAE is evident as the number of FeRh layers increases just beyond the $n = 3$. Obviously, the presence of substitutional Ir atoms enhances the MAE by more than an order of magnitude with respect to the substitution-free FeRh|MgO and clean FeRh films. Since the SOC is proportional to the fourth power of the atomic number, such a large PMA should be attributed to the strength of the SOC of $5d$ orbitals [19]. Previous *ab initio* calculations reported a similar result for the case of clean FeRh films [27]. We here recall that an indication of theoretical prediction [19] has been fully approved in subsequent experiments in which the Ir-capped FeCoB|MgO has the largest PMA ever among the explored TM|FM|MgO multilayers [30]. Thus, we expect that our prediction of the present system would agree, at least in terms of order of magnitude and observed trends, with an experiment. It can be also noted in previous theoretical study that the huge enhancement in MAE and magnetostriction was found in FePt alloys through the Ir substitution for the Pt site [31]. The small deviation in the magnitude and sign of MAE of the substitution-free FeRh in the presence of MgO is

predominantly due to the hybridization between Fe $3d$ and O $2p$ orbitals at the interface [32], which will be clarified later.

In Fig. 2(b) the role of $5d$ SOC effect on the large PMA is further revealed from atom-to-atom decompositions of MAE. The atomic origin of small MAE, 0.25 erg/cm², of the substitution-free FeRh|MgO is the result of the opposite contributions between the Fe and Rh layers at the interface as well as at the surface. The contributions from the center layers are negligible, maintaining the high symmetry bulklike features. For the Ir-substituted FeRh|MgO, it is obvious that the dominant contribution comes solely from the substitutional layer, thus the strong PMA is preserved. The SOC effect as a physics origin of anisotropic phenomena is thus well manifested. Notably, the FM phase at the interface exhibits a trend opposite to the AFM-II phase. The interface Rh layer has negative contribution, whereas it is positive for the AFM-II. This indeed motivates us to explore a crucial effect of the FM instability at the surface on the magnetization switching, as addressed in the forthcoming discussion.

As relative energy, i.e., temperature, increases from the AFM-II [or FM(I)] to the entire FM [or FM(S)], the MAE changes not only in magnitude but also in its sign from positive to negative. Here the phase transition temperature at the AFM \rightarrow FM is qualitatively estimated to be about 360 K from the calculated energy difference of about 31.1 meV/FeRh atom between the AFM(II) and FM phases, which is in the range of experimental values (340–380 K) for FeRh films grown on MgO [11,13]. Importantly, the switching of MAE is quite robust; 6.34 erg/cm² for the low-temperature AFM-II and -5.87 erg/cm² for the high-temperature FM phase, as shown in Fig. 2(c). This implies that, with the presence of Ir substitution, the magnetization direction of FeRh|MgO can be switched and undergoes a transition between perpendicular and in-plane magnetizations at the AFM \rightleftharpoons FM transition, as sketched in Fig. 2(d). It was reported in a previous study that the strain effect during the magnetic transition is responsible for the spin switching of magnetization in substitution-free FeRh films [13]. However, this effect was not taken into account in the present study, which we believe cannot change explicitly our conclusion.

Sign change in MAE of FeRh films in the presence of MgO is analyzed prior to determining the electronic origin of the substitution-induced large PMA. The partial density of states (PDOS) of d orbitals of the Fe [Fe(I)] and Rh atoms [Rh(I)] at the interface, and at the surface layers [Fe(S) and Rh(S)] are shown in Figs. 3(a)–3(d), respectively. From the comparison of the Fe and Rh PDOS, the feature of common peak structures reveals strong orbital hybridization between the Fe $3d$ and Rh $4d$ states, which was considered to play an important role for the magnetic properties of FeRh alloys in the previous experimental and theoretical studies [13,21,27,33]. In particular, the coincidence of simultaneous shifts of Fe and Rh PDOS in the minority spin state towards the high energy level with respect to the corresponding electronic structures in pristine bulk forms is prominent. Due to the Fe-Rh hybridization, for both the Fe(I) and Fe(S) sites the minority spin state of d orbitals is almost unfilled except the $d_{xz,yz}$, whereas the majority spin bands are fully occupied as in pristine Fe films. This significant difference between the spin subbands results in large magnetic moments

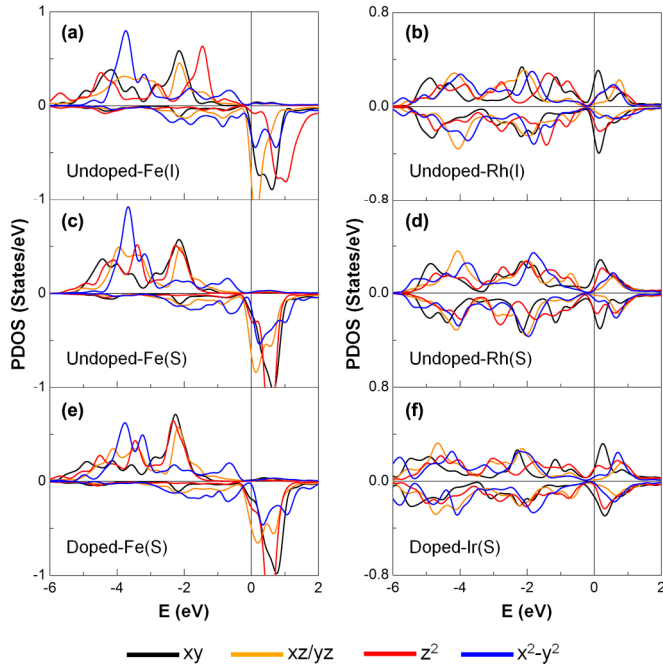


FIG. 3. PDOS of the (a) and (c) Fe and (b) and (d) Rh atoms at the interface and surface layers of the substitution-free FeRh|MgO with $n = 6$, respectively. (e) and (f) The same PDOS for the surface Fe and Ir atoms after Ir substitution. The d_{xy} , $d_{xz/yz}$, d_{z^2} , and $d_{x^2-y^2}$ orbital states are shown in black, orange, red, and blue, respectively. The Fermi level is set to zero energy.

of $3.04 \mu_B$ for the Fe(I) and $3.16 \mu_B$ for the Fe(S) atom. Furthermore, as one goes from the Fe(S) to the Fe(I), the following two features are notable: (1) the $d_{xz,yz}$ peak just above the Fermi level becomes stronger and (2) the minority unoccupied (majority occupied) d_{z^2} states shift upward away from (towards) the Fermi level. The changes of the d_{xy} and $d_{x^2-y^2}$ states are rather featureless, owing to negligible effects of the Fe $3d$ -O $2p$ in-plane orbital hybridization, analogs to the electronic features at the Fe|MgO interface [32,34]. The PDOS of Fe(S) and substitutional Ir(S) atoms for the Ir-substituted FeRh|MgO is also plotted in Figs. 3(e) and 3(f), respectively. Notably, the PDOS of Fe(S) does not differ very much whether the substitutional TM layer underneath the Fe surface is present.

To get more insights, we further decompose the change of MAE distribution on k space of FeRh in the presence of MgO, $\Delta\text{MAE}(k) = \text{MAE}(\text{FeRh|MgO}) - \text{MAE}(\text{FeRh})$, over two-dimensional Brillouin zone (BZ) in Fig. 4(a). Red (orange) area represents negative (positive) MAE(k). The corresponding band structures projected onto five d orbitals for the spin-down state of the Fe(I) and Fe(S) atoms are shown in Figs. 4(c) and 4(e), respectively. For the spin-channel decomposition of MAE, we follow a recipe by the previous full-potential calculations on the free-standing Fe(001) and Fe|MgO films that the spin down-down ($\downarrow\downarrow$) channel contributes much dominantly over the other spin channels, i.e., spin up-down $\uparrow\downarrow$ and up-up $\uparrow\uparrow$ [19,34]. As this argument should be applicable to the present system FeRh|MgO before substitution, owing to the completely filled majority bands (Fig. 3) analogs to the Fe(001) and Fe|MgO, the $\uparrow\downarrow$ and $\uparrow\uparrow$ terms can be simply neglected.

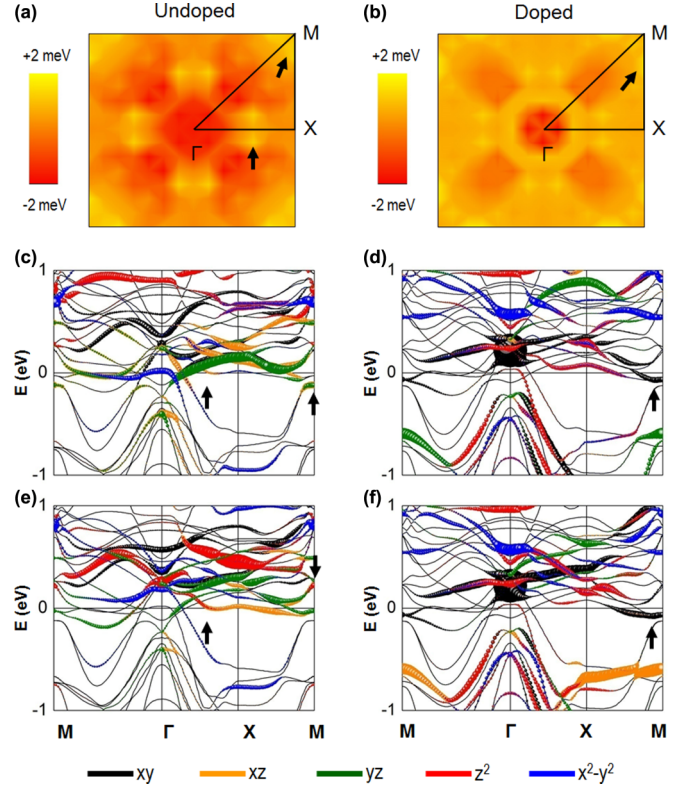


FIG. 4. (a) Change of MAE distribution over k space, $\Delta\text{MAE}(k)$ (in unit of meV), of the FeRh films in the presence of MgO. (b) MAE(k) of the Ir-substituted FeRh|MgO. Orange and red area represent positive and negative MAE(k), respectively. Spin-down band structures of the Fe atoms at the (c) interface and (e) surface layers of the substitution-free FeRh|MgO. (d) Spin-up and (f) spin-down band structures of the substitutional atom of the Ir-substituted FeRh|MgO. The d_{xy} , d_{xz} , d_{yz} , d_{z^2} , and $d_{x^2-y^2}$ orbital states are shown in black, orange, green, red, and blue, respectively. The thin lines represent the energy levels for all atoms in the unit cell, while the broadening of the lines (the size of symbols superimposed over the lines) represents the weight of the Fe and Ir d orbitals.

Within the second-order perturbation theory, the MAE is determined by the SOC between occupied and unoccupied bands as [35]

$$\text{MAE}^{\sigma\sigma'} \approx \xi^2 \sum_{o,u} \frac{|\langle o^\sigma | \ell_z | u^{\sigma'} \rangle|^2 - |\langle o^\sigma | \ell_x | u^{\sigma'} \rangle|^2}{\epsilon_{u,\sigma'} - \epsilon_{o,\sigma}}, \quad (2)$$

where o^σ ($u^{\sigma'}$) and $\epsilon_{o,\sigma}$ ($\epsilon_{u,\sigma'}$) represent eigenstates and eigenvalues of occupied (unoccupied) states for each spin state, $\sigma, \sigma' = \uparrow, \downarrow$, respectively; ξ is the strength of SOC. The total MAE is the sum of Eq. (2) over all atoms in the unit cell. In Eq. (2), the positive and negative contributions to the MAE are characterized by ℓ_z and ℓ_x operators, respectively. Relative contributions of the nonzero ℓ_z and ℓ_x matrix elements are $\langle xz | \ell_z | yz \rangle = 1$, $\langle xy | \ell_z | x^2 - y^2 \rangle = 2$, $\langle z^2 | \ell_x | xz, yz \rangle = \sqrt{3}$, $\langle xy | \ell_x | xz, yz \rangle = 1$, and $\langle x^2 - y^2 | \ell_x | xz, yz \rangle = 1$. For a simple analysis, though all these nonvanishing matrix elements can result in nonnegligible contributions to the MAE, we decompose Eq. (2) into matrix elements with the SOC eigenvalue states that are predominant near the Fermi level in the $\downarrow\downarrow$ component, where the SOC

constant is omitted, as

$$\text{MAE}^{\downarrow\downarrow} = + \frac{|\langle xz|\ell_z|yz\rangle|^2}{\varepsilon_{xz} - \varepsilon_{yz}} - \frac{|\langle xz,yz|\ell_x|z^2\rangle|^2}{\varepsilon_{xz,yz} - \varepsilon_{z^2}}. \quad (3)$$

The band analyses will be concentrated on particular k points at the Γ - X and around the M , indicated by arrows in Figs. 4(c) and 4(e), where the dominant positive contributions of $\text{MAE}(k)$ are prominent [Fig. 4(a)]. For the Fe(I) at the Γ - X , the nondegenerate d_{xz} and d_{yz} bands exist below and above the Fermi level, respectively. This provides the positive contribution in the first term of Eq. (3) through $\langle xz|\ell_z|yz\rangle$ [35]. Similarly, the positive $\text{MAE}(k)$ around the M point comes from the coupling between the d_{xz} and d_{yz} bands across the Fermi level. These bands disappear for the case of Fe(S); instead, the presence of the d_{z^2} state [arrows in Fig. 4(e)], the result of the Fe $3d$ - $O2p$ hybridization as discussed in PDOS in Fig. 3(b), enhances the negative MAE in the second term of Eq. (3), thereby the in-plane magnetization of clean FeRh films. Summing up all these features, one can conclude that the opposite sign in MAE between FeRh films with and without MgO is determined by the competition of SOC states between the first (positive) and second (negative) terms of Eq. (3).

We now explore the large PMA of the Ir-substituted FeRh|MgO, of which the $\text{MAE}(k)$ distribution on full BZ is plotted in Fig. 4(b). The maxima of the positive $\text{MAE}(k)$ mainly appear along the M - X line, which is not present in the substitution-free FeRh|MgO, while the other negative and positive contributions almost remain. As seen in the majority [Fig. 4(d)] and minority [Fig. 4(f)] band plots of the substitutional Ir atom, there are no appreciable coupling of states near the Fermi level throughout the M - Γ - X . Only the SOC pairs between the in-plane orbital characters exist at the X - M in the both spin states. We therefore rewrite Eq. (2) as below, where the other matrix elements vanish,

$$\text{MAE}^{\uparrow\uparrow,\downarrow\downarrow} = + \frac{|\langle xy|\ell_z|x^2 - y^2\rangle|^2}{\varepsilon_{xy} - \varepsilon_{x^2-y^2}}. \quad (4)$$

The SOC coupling between the partially occupied d_{xy} and unoccupied $d_{x^2-y^2}$ states at the M - X predominantly leads to the large PMA of the Ir-substituted FeRh|MgO. This coupling, $\langle xy|\ell_z|x^2 - y^2\rangle$, has the largest contribution to the PMA, by a factor of 2, among the other matrix elements [35]. The same matrix element of Ir atoms was also attributed to be the origin of large MAE and magnetostriction in Ir-substituted FePt alloys, as addressed in previous first-principles calculations [31].

To further signify the importance of the presence of heavy TMs in FeRh|MgO, we explore the other $4d$ and $5d$ substitutions (Ru, Pd, and Pt). From the calculations for the low-temperature AFM-II phase shown in Table I, the magnitude of MAE decreases as the atomic number in $4d$

TABLE I. The calculated MAE (erg/cm²) of the Fe- and TM-terminated FeRh|MgO with $n = 6$ and $n = 6.5$ for their low-temperature phases, respectively.

Termination	Magnetic phase	Ru	Rh	Pd	Ir	Pt
Fe layer	AFM-II	1.99	0.27	0.01	6.34	-0.84
TM layer	FM(S)	2.49	1.71	-0.01	19.36	-7.50

series increases from the Ru to the Pd (almost zero). On the other hand, the spin direction of magnetization changes from the PMA for the Ir to the in-plane in the Pt-substituted FeRh|MgO. These changes in the magnitude and sign of MAE can be explained by the $3d$ - $5d(4d)$ hybridization and the band-filling effects, which were discussed in detail in Ref. [20].

Finally, the possibility of the Rh surface termination is taken into account in accordance with the low-energy electron diffraction experiments under Rh-rich condition [36]. Our total energy calculations in the Rh(Ir)-terminated FeRh|MgO reproduce the previous theoretical results for the clean FeRh films [10]: either AFM-II and FM(I) are not energetically favored regardless of thickness, but a magnetic-phase transition from the entire FM to the FM(S) phase occurs at $n = 3.5$. The GKA superexchange interaction with 180° of Fe-Rh-Fe magnetic coupling cannot be applied to this surface termination due to the absence of Fe layer on the surface. Second, a sufficiently large magnetism (about $1 \mu_B$) of the surface Rh necessitates such stable FM spin orientation within the underneath Fe atoms, as in bulk [9,21]. Not surprisingly, this induced moment is the reflection of a band narrowing due to the reduced dimension, which enhances the DOS at the Fermi level, thereby satisfying the Stoner criteria.

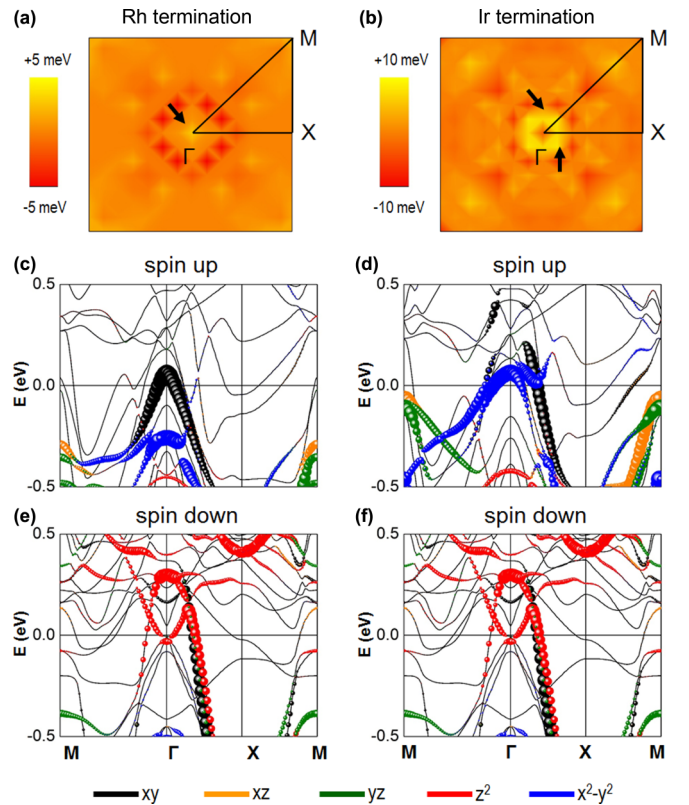


FIG. 5. $\text{MAE}(k)$ (in unit of meV) of the TM-substituted FeRh|MgO films for the (a) Rh and (b) Ir termination. Orange and red areas represent positive and negative $\text{MAE}(k)$, respectively. (c) and (d) Spin-up and (e) and (f) spin-down band structures of the substitutional Rh and Ir atoms at the surface layer of the Rh- and Ir-terminated FeRh|MgO, respectively. The d_{xy} , d_{xz} , d_{yz} , d_{z^2} , and $d_{x^2-y^2}$ orbital states are shown in black, orange, green, red, and blue, respectively. The symbol size represents the weight of the d orbitals.

In general, the presence of TM atoms at the outermost surface (or capping) enhances the MAE significantly, as found for the TM-capped Fe(001) surface [20]. In particular, the Ir (Rh) termination gives rise to a quite strong persistent PMA of 19.36 (1.71) erg/cm² (Table I). This value, to the best of our knowledge, is the largest ever among the reported values today in two- and three-dimensional films. Furthermore, a still large PMA of 1.71 erg/cm² is found for the Rh termination, which agrees with the previous study [27].

The distribution of MAE(*k*) on full BZ is shown for the Rh- and Ir-terminated FeRh|MgO in Figs. 5(a) and 5(b), in which the maxima of the positive MAE(*k*) occur at and around Γ point, respectively. The Γ -centered dominant peak of the positive MAE(*k*) for the Rh termination is attributed to the SOC coupling in the majority spin states of small portion of the dispersive Rh d_{xy} band just above the Fermi level with the occupied $d_{x^2-y^2}$ state at Γ , as shown in Fig. 5(c). For the Ir termination [Fig. 5(d)], these bands move simultaneously upward across the Fermi level, and are completely unoccupied at Γ . As a result, the positive contribution from $\langle xy | \ell_z | x^2 - y^2 \rangle$ is disappeared at Γ , but developed below and above Γ . Hence,

the PMA not only remains but becomes much stronger because of the smaller energy difference between the d_{xy} and $d_{x^2-y^2}$ states in the denominator of Eq. (4). There are no appreciable states that can give positive contribution to the MAE near the Fermi level in the minority spin states for both the Rh and Ir atoms [Figs. 5(e) and 5(f)].

IV. CONCLUSION

In summary, the Rh-site Ir and Rh substitutions nearby the surface of FeRh|MgO lead to a significant enhancement of the PMA in the low-temperature AFM-II phase, which can be further switched into the in-plane magnetization at high-temperature FM phase. While the presence of MgO ignites the FM instability at the interface, the magnetic order in the vicinity of surface as well as the magnitude of PMA decisively depend on the surface termination. In the context of antiferromagnet spintronics, these findings may suggest a feasible approach that yields not only large PMA with low magnetization but also switchable at the AFM \rightleftharpoons FM.

-
- [1] A. D. Kent, *Nat. Mater.* **9**, 699 (2010).
 [2] S. Ikeda *et al.*, *Nat. Mater.* **9**, 721 (2010).
 [3] D. Weller and A. Moser, *IEEE Trans. Magn.* **35**, 4423 (1999).
 [4] J. Z. Sun, *Phys. Rev. B* **62**, 570 (2000).
 [5] A. S. Núñez, R. A. Duine, P. Haney, and A. H. MacDonald, *Phys. Rev. B* **73**, 214426 (2006).
 [6] S. Loth, S. Baumann, C. P. Lutz, D. M. Eigler, and A. J. Heinrich, *Science* **335**, 196 (2012).
 [7] X. Marti *et al.*, *Nat. Mater.* **13**, 367 (2014).
 [8] V. L. Moruzzi and P. M. Marcus, *Phys. Rev. B* **46**, 2864 (1992).
 [9] M. E. Gruner, E. Hoffmann, and P. Entel, *Phys. Rev. B* **67**, 064415 (2003).
 [10] S. Lounis, M. Benakki, and C. Demangeat, *Phys. Rev. B* **67**, 094432 (2003).
 [11] S. Maat, J.-U. Thiele, and E. E. Fullerton, *Phys. Rev. B* **72**, 214432 (2005).
 [12] C. Stamm *et al.*, *Phys. Rev. B* **77**, 184401 (2008).
 [13] C. Bordel, J. Juraszek, D. W. Cooke, C. Baldasseroni, S. Mankovsky, J. Minar, H. Ebert, S. Moyerman, E. E. Fullerton, and F. Hellman, *Phys. Rev. Lett.* **109**, 117201 (2012).
 [14] R. O. Cherifi *et al.*, *Nat. Mater.* **13**, 345 (2014).
 [15] I. Suzuki, M. Itoh, and T. Taniyama, *Appl. Phys. Lett.* **104**, 022401 (2014).
 [16] M. Manekar and S. B. Roy, *J. Phys. D: Appl. Phys.* **41**, 192004 (2008).
 [17] J.-U. Thiele, S. Maat, and E. E. Fullerton, *Appl. Phys. Lett.* **82**, 2859 (2003).
 [18] D. C. Worledge *et al.*, *Appl. Phys. Lett.* **98**, 022501 (2011).
 [19] D. Odkhuu, S. H. Rhim, N. Park, and S. Hong, *Phys. Rev. B* **88**, 184405 (2013).
 [20] D. Odkhuu, S. H. Rhim, N. Park, K. Nakamura, and S. C. Hong, *Phys. Rev. B* **91**, 014437 (2015).
 [21] L. M. Sandratskii and P. Mavropoulos, *Phys. Rev. B* **83**, 174408 (2011).
 [22] R. Y. Gu and V. P. Antropov, *Phys. Rev. B* **72**, 012403 (2005).
 [23] R. Barua, F. Jimnez-Villacorta, and L. H. Lewis, *Appl. Phys. Lett.* **103**, 102407 (2013).
 [24] G. Kresse and J. Hafner, *Phys. Rev. B* **47**, 558 (1993).
 [25] J. P. Perdew, K. Burke, and M. Ernzerhof, *Phys. Rev. Lett.* **77**, 3865 (1996).
 [26] D. D. Koelling and B. N. Harmon, *J. Phys. C* **10**, 3107 (1977).
 [27] S. Jekal, S. H. Rhim, S. C. Hong, W.-j. Son, and A. B. Shick, *Phys. Rev. B* **92**, 064410 (2015).
 [28] C. Baldasseroni *et al.*, *Appl. Phys. Lett.* **100**, 262401 (2012).
 [29] C. J. Kinane *et al.*, *New J. Phys.* **16**, 113073 (2014).
 [30] W. Skowroski, T. Nozaki, Y. Shiota, S. Tamaru, K. Yakushiji, H. Kubota, A. Fukushima, S. Yuasa, and Y. Suzuki, *Appl. Phys. Express* **8**, 053003 (2015).
 [31] D. Odkhuu, W. S. Yun, S. H. Rhim, and S. C. Hong, *Appl. Phys. Lett.* **98**, 152502 (2011).
 [32] H. X. Yang, M. Chshiev, B. Dieny, J. H. Lee, A. Manchon, and K. H. Shin, *Phys. Rev. B* **84**, 054401 (2011).
 [33] Y. Wakisaka, Y. Uemura, T. Yokoyama, H. Asakura, H. Morimoto, M. Tabuchi, D. Ohshima, T. Kato, and S. Iwata, *Phys. Rev. B* **92**, 184408 (2015).
 [34] D. Odkhuu, W. S. Yun, S. H. Rhim, and S. C. Hong (unpublished).
 [35] D. S. Wang, R. Wu, and A. J. Freeman, *Phys. Rev. B* **47**, 14932 (1993).
 [36] S. Kim, F. Jona, and P. M. Marcus, *Surf. Rev. Lett.* **6**, 133 (1999).